Fracture of anisotropic materials with plastic strain-gradient effects

Brian Nyvang Legarth[1,*]

[1] Department of Mechanical Engineering, Solid Mechanics,
Technical University of Denmark, DK-2800, Denmark
* Corresponding author: bnl@mek.dtu.dk

Abstract A unit cell is adopted to numerically analyze the effect of plastic anisotropy on fracture evolution in a micro-reinforced fiber-composite. The matrix material exhibit size-effects and an anisotropic strain-gradient plasticity model accounting for such size-effects through a material length scale parameter is adopted. The fracture process along the fiber-matrix interface is modeled using a recently proposed cohesive law extension having an additional material length parameter. Due to the fiber-matrix fracture a sudden stress-drop is seen in the macroscopic stress-strain response which defines the failure strain of the composite. The effect of the two material length parameters on the failure strain of the composite is studied. For small values of the material length scale parameter conventional predictions are obtained. Larger values of the material length scale parameter result in corresponding larger failure strains, but only up to a material length scale parameter approximately equal to 15% of the reinforcement size. At this point, the failure strain becomes smaller again for further increasing values of the material length scale. It is shown that the cohesive length parameter monotonically affects the failure strain as a decreasing failure strain is predicted for smaller value of the material parameter.

Keywords Composite Materials, Strain-gradient plasticity, Debonding, Failure strain

1. Introduction

Failure mechanisms of fiber-reinforced composite materials are still a challenging topic due to the large number of failure modes compared to conventional homogeneous materials[1]. A unidirectional fiber-composite subjected to transverse tensile loading often fail by either matrix damage or microcracks evolving at the fiber-matrix interfaces. For longitudinal loading the most often seen failure modes are matrix and fiber cracking.

For a composite reinforced at the micron scale, two competing mechanisms affect the overall behavior: (I) interfacial failure reduces the strength and (II) strain-gradient effects enhance the strength. When analyzing such composites in general a full 3D analysis is required in order to fully represent the geometry, the loading and the boundary conditions. Such analyses are complicated and the computations become very time consuming when anisotropic plasticity and progressive debonding is to be accounted for. Thus, assuming a periodical distribution of the reinforcement allows for greatly simplified approaches.
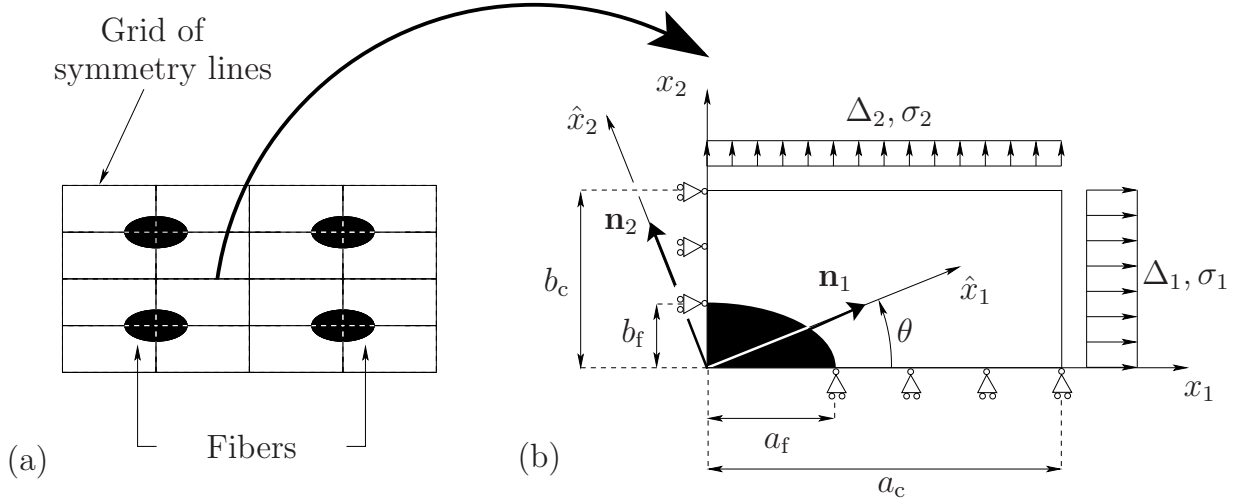
Figure 1. The plane strain cell model for the composite. (a) Periodically distributed fibers. (b) The cell used for modeling with initial dimensions, loads, supports and coordinate systems.

Here, a composite material having a periodical distribution of reinforcement is analyzed using a plane strain unit cell approach. Thus, the results presented in this study approximate a composite of rather long, almost aligned, stiff reinforcement which is subjected to a fixed stress state that is acting mainly in the transverse direction of the reinforcement. Fig. 1(a) shows the distribution of fibers and Fig. 1(b) shows the unit cell adopted here. The orthonormal basis, $\mathbf{n}_i$, of the principal axes of plastic anisotropy, $\hat{x}_i$, is defined by the angle θ, from from the global Cartesian coordinate system, x_i. The applied conventional boundary conditions are

$$
\begin{aligned}
\dot{u}_1 = 0, \;\; \dot{T}_2 = 0 \;\; \text{on} \;\; x_1 = 0 \;\; \text{and} \;\; \dot{u}_1 = \Delta_1, \;\; \dot{T}_2 = 0 \;\; \text{on} \;\; x_1 = a_c \\
\dot{u}_2 = 0, \;\; \dot{T}_1 = 0 \;\; \text{on} \;\; x_2 = 0 \;\; \text{and} \;\; \dot{u}_2 = \Delta_2, \;\; \dot{T}_1 = 0 \;\; \text{on} \;\; x_2 = b_c
\end{aligned}
\tag{1}
$$

where u_i are the displacement components, Δ_1 and Δ_2 are displacement increment quantities on two sides of the cell, which are calculated such that the ratio of the average true stresses σ_2 and σ_1 remains fixed, $\sigma_2/\sigma_1 = \kappa$. These stresses are calculated as

$$
\begin{aligned}
\sigma_1 = \tfrac{1}{b_c + \Delta b_c} \int_0^{b_c + \Delta b_c} [T_1]_{x_1 = a_c + \Delta a_c} \, dx_2 \\
\sigma_2 = \tfrac{1}{a_c + \Delta a_c} \int_0^{a_c + \Delta a_c} [T_2]_{x_2 = b_c + \Delta b_c} \, dx_1
\end{aligned}
\tag{2}
$$

Here Δa_c and Δb_c denote the accumulated elongations of the cell sides whereas T_1 and T_2 are normal tractions. The corresponding average logarithmic strains are

$$
\begin{aligned}
\epsilon_1 = \ln(1 + \Delta a_c / a_c) \\
\epsilon_2 = \ln(1 + \Delta b_c / b_c)
\end{aligned}
\tag{3}
$$

In this study, a micro-crack evolving at the fiber-matrix interfaces is analyzed for a two-phase composite material, where the matrix material exhibits size-effects. The higher-order strain-gradient plasticity model of Fleck and Hutchinson accounts for such size-effects and will be adopted here in the anisoropic version proposed by Legarth [2,3]. In this model a higher-order stress work-conjugate to the gradient of the effective plastic strain is introduced together with a material length scale parameter. The reinforcement is assumed to be much stiffer than the matrix material and will therefore be considered as perfectly stiff. As dislocations cannot penetrate into the perfectly elastic fiber they pile up

at the interface which corresponds to zero plastic deformations. Thus, zero plastic strain is imposed at the bonded part of the interface. This is known a higher-order boundary conditions. The fracture process along the fiber-matrix interface is modelled using a recently proposed cohesive law extension[4]. Hence, plasticity will affect the fracture process as both the average as well as the jump in plastic strain across the fiber-matrix interface are taking into account in this cohesive law. Using this extended cohesive law ensures stress-free crack faces after failure. The formulation used here only demands one additional interfacial cohesive zone parameter.

2. Material models

The material model used accounts for small elastic and finite plastic strain in an updated Lagrangian formulation in which the current configuration is taken as the reference configuration, i.e. $J = 1$ but $\dot{J} = \dot{\epsilon}_{kk}$ when J is the determinant of the metric tensor and the superposed dot denotes the time rate.

2.1 Higher order elasto-plastic constitutive model

The fibers are assumed to be purely elastic with a stiffness much larger than the elasto-plastic matrix material, which is assumed to obey the strain gradient model proposed by Fleck and Hutchinson [2]. Denoting the velocity field $\dot{u}_i$ the components of the second-order velocity gradient tensor, $\dot{e}_{ij}$, are determined by $\dot{e}_{ij} = \dot{u}_{i,j}$. The symmetric part of $\dot{e}_{ij}$ is the strain rate, $\dot{\epsilon}_{ij}$, and the antisymmetric part is the continuum spin tensor, $\dot{\omega}_{ij}$. Following the multiplicative decomposition of the deformation gradient into an elastic and a plastic part the kinematics of the material can be written as

$$
\begin{aligned}
\dot{\epsilon}_{ij} &= \tfrac{1}{2}(\dot{e}_{ij} + \dot{e}_{ji}) = \dot{\epsilon}_{ij}^{\mathrm{e}} + \dot{\epsilon}_{ij}^{\mathrm{P}} \\
\dot{\omega}_{ij} &= \tfrac{1}{2}(\dot{e}_{ij} - \dot{e}_{ji})
\end{aligned}
\tag{4}
$$

with $\dot{e}_{ij} = \dot{\epsilon}_{ij} + \dot{\omega}_{ij}$ and e and p denote the elastic and the plastic parts, respectively.

Plastic anisotropy is accounted for using the anisotropic version of the Fleck and Hutchinson model as suggested by Legarth [3]. Thus, the effective plastic strain, $\dot{E}^p$, is enriched by the gradients of the conventional effective plastic strain, $\dot{\epsilon}_{,i}^{p}$, and a material length scale parameter, l_*, as

$$
\dot{E}^p = \sqrt{\frac{2}{3}\dot{\epsilon}_{ij}^p \dot{\epsilon}_{ij}^p + l_*^2 \dot{\epsilon}_{,i}^{p}\,\dot{\epsilon}_{,i}^{p}} \quad ; \quad \dot{\epsilon}_{ij}^p = \dot{\epsilon}^p N_{ij}^p = \dot{\epsilon}^p \frac{\partial \Gamma}{\partial \sigma_{ij}} \quad ; \quad \dot{\epsilon}^p = \sqrt{\frac{2}{3}\dot{\epsilon}_{ij}^p \dot{\epsilon}_{ij}^p} \tag{5}
$$

The work-conjugate effective stress is denoted σ_c and is given in Tab. 1 for the four posible cases of isotropy or anisotropy with and without strain gradient effects. Plastic anisotropy enters through the effective stress measure Γ whereas the higher-order stress, ρ_i, relates to the strain-gradient effects as the work-conjugate stress quantity to the gradient of the plastic strain rate, $\dot{\epsilon}_{,i}^{p}$. The work-conjugate stress quantity to the effective plastic strain rate, $\dot{\epsilon}^p$ is denoted q.

Two different anisotropic yield surfaces are adopted here, namely the classical anisotropic Hill yield surface [5] and the more recent non-quadratic proposal by Barlat et al. [6], here denoted Hill-48 and Barlat-91, respectively.

Table 1. Summary of the effective stress, σ_c, for different materials.

	Conventional materials $(l_* = 0, \rho_i = 0)$	Higher order materials $(l_* \neq 0, \rho_i \neq 0)$
Isotropic	$\rho_{i,i} = 0$	$\rho_{i,i} = q - \sigma_\mathrm{e}$
$(\Gamma = \sigma_\mathrm{e})$	$\sigma_\mathrm{c} = \sigma_\mathrm{e}$	$\sigma_\mathrm{c} = \sqrt{(\sigma_\mathrm{e} + \rho_{i,i})^2 + l_*^{-2}\rho_i\rho_i}$
Anisotropic	$\rho_{i,i} = 0$	$\rho_{i,i} = q - \Gamma$
	$\sigma_\mathrm{c} = \Gamma$	$\sigma_\mathrm{c} = \sqrt{(\Gamma + \rho_{i,i})^2 + l_*^{-2}\rho_i\rho_i}$

Hill-48

For the case of plane strain conditions with $\sigma_{13} = \sigma_{23} = 0$ the yield surface of Hill is

$$\Gamma = \sqrt{\tfrac{3}{2(F+G+H)} \left[F(\hat{\sigma}_{22} - \hat{\sigma}_{33})^2 + G(\hat{\sigma}_{33} - \hat{\sigma}_{11})^2 + H(\hat{\sigma}_{11} - \hat{\sigma}_{22})^2 + 2N\hat{\sigma}_{12}^2 \right]} \qquad (6)$$

The Cauchy stresses, $\hat{\sigma}_{ij}$, refer to the principal axes of plastic anisotropy. For $F = G = H = 1$ and $N = L = M = 3$, Eq. (6) equals the isotropic Mises yield surface, σ_e.

Barlat-91

Barlat et al. [5] proposed the non-quadratic yield function

$$\Gamma = [S_1 - S_2]^d + [S_2 - S_3]^d + [S_1 - S_3]^d \qquad (7)$$

where

$$\begin{aligned}
S_1 &= 2\sqrt{I_2}\cos\left(\tfrac{\bar{\theta}}{3}\right) \\
S_2 &= 2\sqrt{I_2}\cos\left(\tfrac{\bar{\theta}-2\pi}{3}\right) \\
S_3 &= 2\sqrt{I_2}\cos\left(\tfrac{\bar{\theta}+2\pi}{3}\right)
\end{aligned} \qquad (8)$$

$$\begin{aligned}
I_2 &= \tfrac{1}{3}\left[(\bar{f}\bar{F})^2 + (\bar{g}\bar{G})^2 + (\bar{h}\bar{H})^2\right] \\
&\quad + \tfrac{1}{54}\left[(\bar{a}\bar{A} - \bar{c}\bar{C})^2 + (\bar{c}\bar{C} - \bar{b}\bar{B})^2 + (\bar{b}\bar{B} - \bar{a}\bar{A})^2\right] \\[6pt]
I_3 &= \tfrac{1}{54}\left[(\bar{c}\bar{C} - \bar{b}\bar{B})(\bar{a}\bar{A} - \bar{c}\bar{C})(\bar{b}\bar{B} - \bar{a}\bar{A})\right] + \bar{f}\bar{g}\bar{h}\bar{F}\bar{G}\bar{H} \\
&\quad - \tfrac{1}{6}\left[(\bar{c}\bar{C} - \bar{b}\bar{B})(\bar{f}\bar{F})^2 + (\bar{a}\bar{A} - \bar{c}\bar{C})(\bar{g}\bar{G})^2 + (\bar{b}\bar{B} - \bar{a}\bar{A})(\bar{h}\bar{H})^2\right]
\end{aligned} \qquad (9)$$

$$0 \leq \bar{\theta} = \arccos\left(\frac{I_3}{I_2^{3/2}}\right) \leq \pi \qquad (10)$$

with

$$\begin{aligned}
\bar{A} &= \hat{\sigma}_{22} - \hat{\sigma}_{33} &;&\quad \bar{F} &= \hat{\sigma}_{23} \\
\bar{B} &= \hat{\sigma}_{33} - \hat{\sigma}_{11} &;&\quad \bar{G} &= \hat{\sigma}_{31} \\
\bar{C} &= \hat{\sigma}_{11} - \hat{\sigma}_{22} &;&\quad \bar{H} &= \hat{\sigma}_{12}
\end{aligned} \qquad (11)$$

For $\bar{\theta} = 0$ or $\bar{\theta} = \pi$ in Eq. (10) the derivatives in Eq. (5) are singular. For these particular cases Eq. (7) reduces to

$$\Gamma = 2 \cdot 3^d I_2^{\frac{d}{2}} \qquad \text{for } \bar{\theta} = 0 \quad \text{or} \quad \bar{\theta} = \pi \qquad (12)$$

which are then directly used to evaluate the strain increments. If the coefficients of anisotropy, $\bar{a}, \bar{b}, \bar{c}, \bar{f}, \bar{g}$ and $\bar{h}$, are chosen to be unity and the exponent to $d = 2$, this criterion reduces to the von Mises yield surface.

4

2.2 Higher-order cohesive model

The bi-axial loading on the unit cell, Fig. 1(b), will tend to cause both normal and tangential interfacial separation, u_n and u_t, respectively, at the fiber-matrix interface. The cohesive zone model proposed by Tvergaard[7] takes both types of separation into account and therefore this model may seem suitable for the present study. However, due to the existence of the higher order stress, ρ_i with the corresponding higher order tractions, $\rho_i n_i$ additional terms need to be included in order to have a conventional as well as higher order stress-free surface after debonding failure. Hence, a non-dimensional damage parameter is introduces as[4]

$$\lambda = \sqrt{\left(\frac{u_n}{\delta_n}\right)^2 + \left(\frac{u_t}{\delta_t}\right)^2 + l_*^2 \left[\left(\frac{<\epsilon^p>}{l_A}\right)^2 + \left(\frac{[\epsilon^p]}{l_J}\right)^2\right]} \tag{13}$$

where $<\epsilon^p>$ is the average (subscript A) and $[\epsilon^p]$ is the half jump (subscript J) in plastic strain across the interface, respectively, whereas l_A and l_J are corresponding critical interfacial length scale parameters. For $\lambda \geq 1$ total separation have occurred. It is noted, that since the fiber is taken to be purely elastic in this study the average plastic strain across the fiber-matrix interface equals the jump, i.e. $<\epsilon^p> = [\epsilon^p]$. The corresponding tractions are

$$T_n = \frac{u_n}{\delta_n}F(\lambda) \; ; \quad T_t = \alpha\frac{u_t}{\delta_t}F(\lambda) \; ; \quad T_A = l_*^2\frac{\delta_n}{l_A^2}F(\lambda)<\epsilon^p> \; ; \quad T_J = l_*^2\frac{\delta_n}{l_J^2}F(\lambda)[\epsilon^p] \tag{14}$$

with $\alpha = \delta_n/\delta_t$ and $F(\lambda) = \frac{27}{4}\sigma_{max}(1 - 2\lambda + \lambda^2)$ for $0 \leq \lambda \leq 1$. The maximum interfacial stress is denoted σ_{max}. For the numerical implementation, an incremental version of these tractions can be stated generally as

$$\left\{\begin{array}{c} \dot{T}_n \\ \dot{T}_t \\ \dot{T}_A \\ \dot{T}_J \end{array}\right\} = \left[\begin{array}{cccc} a_{nn} & a_{nt} & a_{nJ} & a_{nA} \\ a_{tn} & a_{tt} & a_{tJ} & a_{tA} \\ a_{Jn} & a_{Jt} & a_{JJ} & a_{JA} \\ a_{An} & a_{At} & a_{AJ} & a_{AA} \end{array}\right] \left\{\begin{array}{c} \dot{u}_n \\ \dot{u}_t \\ [\dot{\epsilon}^p] \\ <\dot{\epsilon}^p> \end{array}\right\} \tag{15}$$

where the a-coefficients can be found from the cohesive law. Using this higher order cohesive law ensures that the debonded part of the fiber-matrix interface is stress free both in terms of the conventional stress, σ_{ij}, as well as the higher order stress, ρ_i.

3. Computational Method

The problem is solved incrementally by a finite element code based on the principle of virtual work. In the updated Lagrangian formulation the incremental form of the principle of virtual work is, see [3,5]

$$\Delta t \int_V \left(\overset{\triangledown}{\varsigma}_{ij}\,\delta\dot{\epsilon}_{ij} - \sigma_{ij}(2\dot{\epsilon}_{ik}\delta\dot{\epsilon}_{kj} - \dot{e}_{kj}\delta\dot{e}_{ki}) + \left(\dot{q} - \dot{\Gamma}^\varsigma\right)\delta\dot{\epsilon}^P + \overset{\vee}{\rho}_i\,\delta\dot{\epsilon}^P_{,i}\right)dV$$
$$+\Delta t \int_{S_I}\left(\dot{T}_n\delta\dot{u}_n + \dot{T}_t\delta\dot{u}_t + \dot{p}\delta[\dot{\epsilon}^P] + \dot{q}\delta<\dot{\epsilon}^P>\right)dS = \Delta t \int_S\left(\dot{T}_i\delta\dot{u}_i + \dot{\rho}_i n_i\delta\dot{\epsilon}^P\right)dS \tag{16}$$

Here, Δt is the time step, V the volume, $\overset{\triangledown}{\varsigma}_{ij}$ denotes the Jaumann rate of the Kirchhoff stress with $\dot{\Gamma}^\varsigma = N_{ij}^P\,\overset{\triangledown}{\varsigma}_{ij}$ and $T_i = \sigma_{ij}n_j$ are the surface tractions on the surface S with

the unit outward normal n_i. Due to the updated Lagrangian formulation all integrations are carried out in the current deformed configuration. The Jaumann rate of the Kirchhoff stress entering the virtual work principle is

$$\overset{\triangledown}{\varsigma}_{ij}\,\Delta t = R_{ijkl}\left(\Delta\epsilon_{kl} - N_{kl}^{\mathrm{P}}\Delta\epsilon^{\mathrm{P}}\right) = \Delta\varsigma_{ij} - \Delta\omega_{ik}\sigma_{kj} - \sigma_{ik}\Delta\omega_{jk} \tag{17}$$

where R_{ijkl} are the isotropic elastic moduli determined by Young's modulus, E, Poisson's ratio, ν, and Kronecker's delta, δ_{ij}, as

$$R_{ijkl} = \frac{E}{1+\nu}\left(\frac{1}{2}(\delta_{ik}\delta_{jl} + \delta_{il}\delta_{jk}) + \frac{\nu}{1-2\nu}\delta_{ij}\delta_{kl}\right) \tag{18}$$

The finite element procedure adopted here follows the method used by de Borst and Pamin[8] for time-independent plasticity and Borg et al.[9] for viscoplasticity, where both the conventional displacement increments, $\mathbf{\Delta D}$, as well as the increments of the effective plastic strain rates, $\mathbf{\Delta}\dot{\epsilon}^{\mathrm{p}}$, appear as unknowns. However, they solved for $\mathbf{\Delta D}$ and $\mathbf{\Delta}\dot{\epsilon}^{\mathrm{p}}$ simultaneously, even though the system of equations decouples. Here, the numerical solution is obtained by decoupling the equations. In doing so, the stiffness matrices become symmetric, less sparse and more well conditioned, leading to a significantly improved computational time. Thus, the equations to solve are

$$\mathrm{K}_{\mathrm{e}}\mathbf{\Delta D} = \mathbf{\Delta F}_1 + \mathbf{\Delta F}_{1c} \tag{19}$$

for the displacement increments and

$$\mathrm{K}_{\mathrm{p}}\mathbf{\Delta}\dot{\epsilon}^{\mathrm{P}} = \mathbf{\Delta F}_2 + \mathbf{\Delta F}_{2c} \tag{20}$$

for the increments of the conventional effective plastic strain rate. Here 8 node isoparametric elements are used for both the displacements as well as the plastic strain field using the shape functions N and M, respectively, within the bulk material. Thus, the field of total strains within an element is bi-linear whereas the plastic strains vary parabolically. The local stiffness matrices and load vectors are

$$\begin{aligned}
\mathrm{K}_{\mathrm{e}}^{NM} = \quad &\int_V \left(E_{ij}^N R_{ijkl}E_{kl}^M + \sigma_{ij}\left(N_{k,j}^M N_{k,i}^N - 2E_{ik}^M E_{jk}^N\right)\right)\mathrm{d}V + \\
&\int_{S_I}\left(\{a_{nn}(Q_i^N n_i) + a_{nt}(Q_i^N t_i)\}(Q_i^M n_i) + \right. \\
&\left.\{a_{tn}(Q_i^N n_i) + a_{tt}(Q_i^N t_i)\}(Q_i^M t_i)\right)\mathrm{d}S
\end{aligned} \tag{21}$$

$$\begin{aligned}
\mathrm{K}_{\mathrm{P}}^{NM} = \quad &\int_V \left(\left(\frac{\dot{\epsilon}^{\mathrm{P}}}{\dot{E}^{\mathrm{P}2}}(m-1)q + \frac{\sigma_{\mathrm{c}}}{\dot{E}^{\mathrm{P}}}\right)M^M M^N \right. \\
&+ l_*^2\frac{\dot{\epsilon}_{,i}^{\mathrm{P}}}{\dot{E}^{\mathrm{P}2}}qM^M M_{,i}^N + \frac{\dot{\epsilon}^{\mathrm{P}}}{\dot{E}^{\mathrm{P}2}}(m-1)\rho_i M_{,i}^M M^N \\
&\left. + l_*^2\frac{\dot{\epsilon}_{,i}^{\mathrm{P}}}{\dot{E}^{\mathrm{P}2}}\rho_k M_{,k}^M M_{,i}^N + \frac{\sigma_{\mathrm{c}}}{\dot{E}^{\mathrm{P}}}M_{,i}^M M_{,i}^N\right)\mathrm{d}V
\end{aligned} \tag{22}$$

$$\mathbf{\Delta F}_1^N = \quad \int_S \Delta T_i N_i^N \mathrm{d}S + \Delta t\int_V E_{ij}^N R_{ijkl}N_{kl}^{\mathrm{P}}\dot{\epsilon}^{\mathrm{P}}\mathrm{d}V \tag{23}$$

$$\begin{aligned}
\mathbf{\Delta F}_2^N = \quad &\int_S \Delta\rho_i n_i M^N \mathrm{d}S - \Delta t\int_V \left(\left(N_{ij}^{\mathrm{P}}R_{ijkl}(N_{kl}^{\mathrm{P}}\dot{\epsilon}^{\mathrm{P}} - \dot{\epsilon}_{kl})\right.\right. \\
&\left.\left. + \frac{\dot{\epsilon}^{\mathrm{P}}}{\dot{\epsilon}_0^m}\dot{E}^{\mathrm{P}m}\frac{\mathrm{d}g}{\mathrm{d}E^{\mathrm{P}}}\right)M^N + \dot{\epsilon}_{,i}^{\mathrm{P}}\,\dot{E}^{\mathrm{P}m}\frac{\mathrm{d}g}{\mathrm{d}E^{\mathrm{P}}}\frac{l_*^2}{\dot{\epsilon}_0^m}M_{,i}^N\right)\mathrm{d}V
\end{aligned} \tag{24}$$

where $E_{ij} = \frac{1}{2}\left(N_{i,j} + N_{j,i}\right)$ and m is the rate sensitivity parameter. The additional load vectors $\mathbf{\Delta F}_{1c}$ and $\mathbf{\Delta F}_{2c}$ resulting from the higher order cohesive zone are

$$\begin{aligned}
\mathbf{\Delta F}_{1c}^N = \quad &-\Delta t\int_{S_I}\left(\{a_{nJ}[\dot{\epsilon}^p] + a_{nA} <\dot{\epsilon}^p>\}(Q_i^N n_i) \quad + \right. \\
&\left.\{a_{tJ}[\dot{\epsilon}^p] + a_{tA} <\dot{\epsilon}^p>\}(Q_i^N t_i)\right)\mathrm{d}S
\end{aligned} \tag{25}$$

$$\begin{aligned}
\mathbf{\Delta F}_{2c}^N = \quad &-\Delta t\int_{S_I}\left(a_{Jn}\dot{u}_n + a_{Jt}\dot{u}_t + a_{JJ}[\dot{\epsilon}^p] + a_{JA} <\dot{\epsilon}^p> \quad + \right. \\
&\left. a_{An}\dot{u}_n + a_{At}\dot{u}_t + a_{AJ}[\dot{\epsilon}^p] + a_{AA} <\dot{\epsilon}^p>\right)R^N \mathrm{d}S
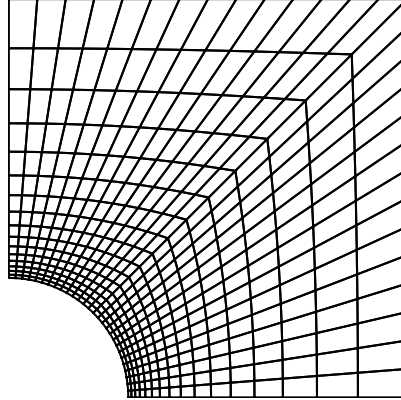\end{aligned} \tag{26}$$

Figure 2. Example of mesh adopted.

Here, 6 node isoparametric elements with the shape functions Q and R for the displacement field and the plastic strain field, respectively, are used for the cohesive zone where the normal and tangential unit vectors are introduced as n_i and t_i, respectively. It noted that the incremental cohesive tractions, Eq. (15), depends on the rates of the displacement and the plastic strain, whereas the solution procedure outlined here solves for the rates of the displacement and the plastic strain increments, meaning that the higher order contributions from the cohesive law only enters through the load vectors, ΔF_{1c} and ΔF_{2c}. The conventional part of the cohesive law also gives an stiffness contribution, Eq. (21). An example of a mesh used is shown in Fig. 2 for $\frac{a_f}{b_f} = \frac{a_c}{b_c} = 1$.

4. Results

Fig. 3 shows results for a load case with $\kappa = \frac{\sigma_2}{\sigma_1} = 0.5$ corresponding to bi-axial plane strain tension. The fiber volume fraction is $V_f = \frac{\pi a_f b_f}{4 a_c b_c}$, with $\frac{a_f}{b_f} = \frac{a_c}{b_c} = 1$. The initial yield stress is $\sigma_0/E = 0.003$, where E is Young's modulus. The coefficients of anisotropy using Hill-48 are $F = 0.7, G = 3.33, H = 1$ and $N = 9.6$ with $\theta = 0^o$ and $\sigma_{max} = 3\sigma_0$.
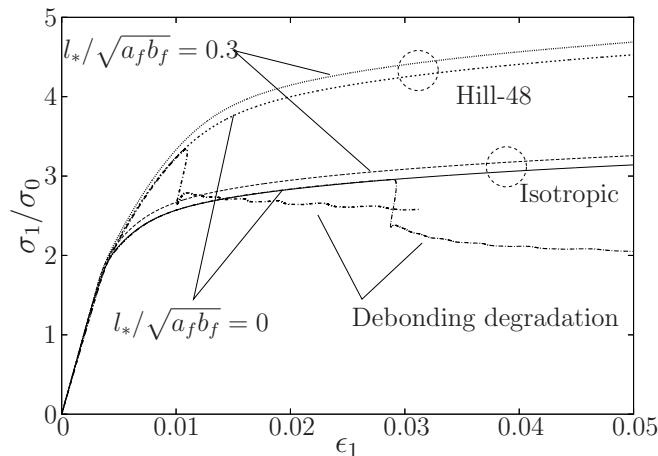

Figure 3. Bi-axial tension results, $\kappa = 0.5$, for isotropy and Hill-48 anisotropy. (a) Average stress-strain curves, Eqs. (2) and (3). (b) Contours of effective plastic strain for a conventional anisotropic material with debonding (c) Contours of effective plastic strain for a higher order anisotropic material without debonding.

7

For both isotropic and anisotropic behavior the effect of the material length scale parameter, l_*, is an increased load carrying capacity. A sudden stress drop occurs due to debonding which defines the failure strain of the composite, ϵ^f. In Fig. 4 this failure strain is plottet as function of the normalized material length scale parameter of the matrix material, $l_*/\sqrt{a_f b_f}$. It is seen, that the failure strain, ϵ^f, does not vary monotonically by the material length scale parameter, l_*, but reaches a maximum approximately for $l_*/\sqrt{a_f b_f} = 0.15$.
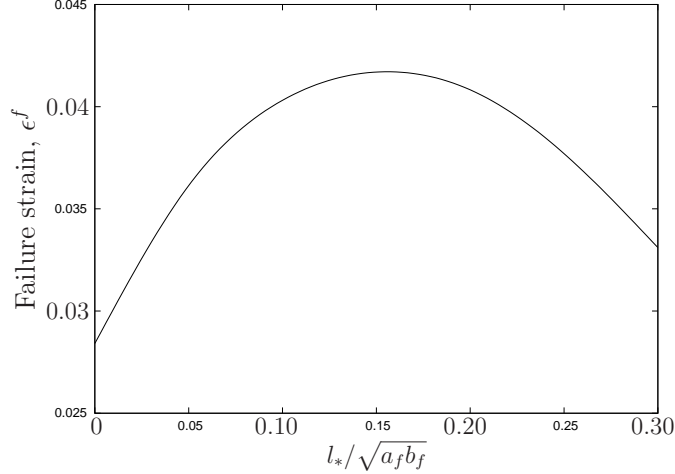
Figure 4. The failure strain as function of the material length scale parameter, l_*, normalized against the fiber radius, R. Isotropic results are shown for $\kappa = 0.5$.

On the other hand, a monotonic effect on the failure strain is found when studying the influence of the length scale parameter of the cohesive law, $l_A = l_J$ in Eq. (13). Fig. 5 shows the failure strain as function of the new cohesive length scale parameter, L_J, normalized against the matrix material length scale parameter, l_*. Both isotropic results as well as anisotropic results are shown using Hill-48 as well as Barlat-91. The coefficients of Barlat-91 are chosen such that the same plastic anisotropy as modeled by Hill-48 is reproduced. Thus, the two anisoropic results are directly comparable.
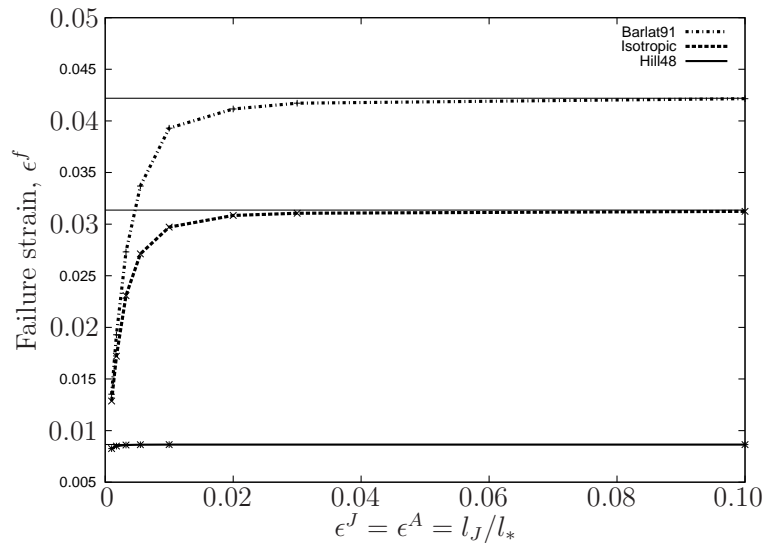

Figure 5. The failure strain as function of the cohesive length scale parameter, L_J, normalized by the matrix material length scale parameter, l_*. Isotropic as well as anisotropic results are shown for $\kappa = 0.5$.

Compared to isotopy, the failure strain is larger using Barlat-91 and smaller using Hill-48. However, a significant effect of $l_J/l_* = l_A/l_*$ is seen for decreasing values as the failure strain decreases as well. On the other hand, for increasing larger l_J-values the plastic behaviour of the cohesive law is supressed and conventional results are obtained as shown by the asymptotic lines. For the Hill material the effect is very small, as debonding failure occurs at a rather small plastic strain, see Fig. 3. Thus, the influence of plasticity in the cohesive law is limited.

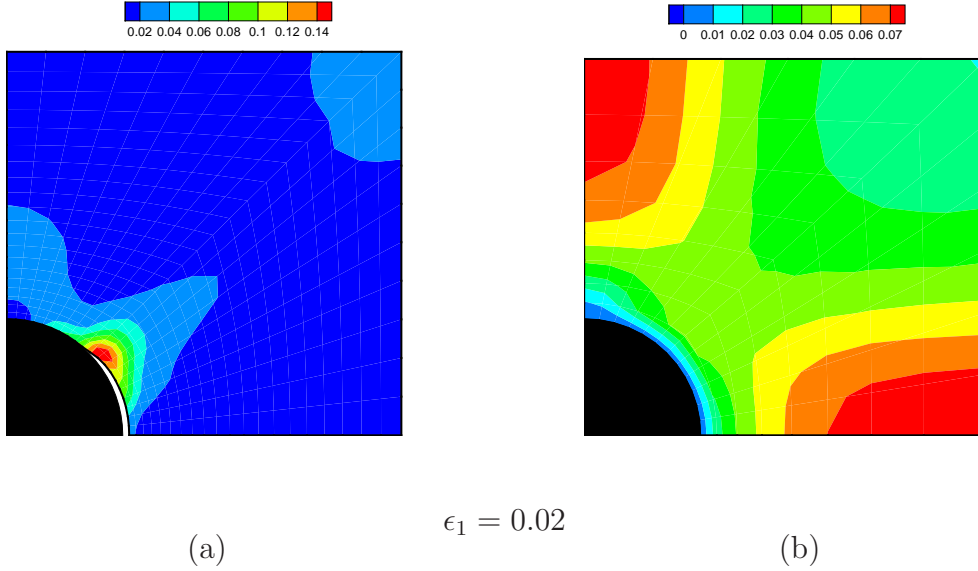$$\epsilon_1 = 0.02$$

(a)   (b)

Figure 6. Bi-axial tension results, $\kappa = 0.5$, for Hill-48 anisotropy at $\epsilon_1 = 0.02$. (a) Contours of effective plastic strain for a conventional anisotropic material with debonding (b) Contours of effective plastic strain for a higher order anisotropic material without debonding.

In Fig. 6(a) the micro-crack evolving at the fiber-matrix interface can be seen and the contours of the effective plastic strain shows severe strain with larger gradient at the crack-tip. Such large gradients are costly if strain-gradient effects are accounted for. Fig. 6(b) illustrates this for a case where a micro-crack has not evolved but the strain field is much more smooth. It can also be seen that the plastic strain near the fiber-matrix interface vanishes due to the imposed boundary conditions.

5. Conclusion

In conclusion, this study analyzes numerically the combined effects of plastic anisotropy, size-effects and debonding in a composite material. Debonding is seen as a sudden stress drop and plastic anisotropy highly affects the failure strain, while the size-effect is observed as an increased load carrying capacity. The material length scale of the cohesive law tends to reduce the failure strain of the composite, but as the parameter becomes sufficient large conventional results are predicted. This holds for both isotropic as well as anisotropic materials. The material length scale of the matrix material shows a non-monotonic effect on the failure strain such that a maximum failure strain is predicted for approximately a material length scale parameter of 15% of the fiber radius.

References

[1] Talreja R. Damage analysis for structural integrity and durability of composite materials, Fatigue Fract Engng. Mater. Struct., 29, 481-506, 2005.

[2] Fleck. N. A., Hutchinson, J. W.: A reformulation of strain gradient plasticity. J. of the. Mech. and Phys. of Solids, 49, 2245-2271, 2001.

[3] Legarth, B. N.: Strain-gradient effects in anisotropic materials. Model. and Sim. in Mater. Sci. and Eng. 15, S71-S81, 2007.

[4] Niordson, C. F.: Cohesive element for Fleck & Hutchinson 2001. Technical report, Technical University of Denmark, 2010.

[5] Hill, R.: A theory of the yielding and plastic flow of anisotropic metals. Proc. Royal Soc. London. A193, 281-297, 1948.

[6] Barlat, F., Lege, D.J. and Brem, J.C.: A six-component yield function for anisotropic materials. Int. J. Plast. 7, 693-712, 1991.

[7] Tvergaard, V.: Effect of fibre debonding in a whisker-reinforced metal. Mater. Sci. & Eng. A125, 203-213, 1990.

[8] Borg. U, Niordson, C. F., Fleck. N. A., Tvergaard, V.: A viscoplastic strain gradient analysis of materials with voids or inclusions. Int. J. Solids Struct, 43, 4906-4916, 2006.

[9] de Borst, R. Pamin, J.: Some novel developments in finite element procedures for gradient-dependent plasticity. Int. J. Num. Meth. Eng. 39(14), 2477-2505, 1996.

Acknowlegdment